Hindawi Publishing Corporation
Mathematical Problems in Engineering
Volume 2015, Article ID 635395, 14 pages
http://dx.doi.org/10.1155/2015/635395

Research Article

Trajectory Optimization for a Cruising Unmanned Aerial Vehicle Attacking a Target at Back Slope While Subjected to a Wind Gradient

Tieying Jiang,[1] Jie Li,[1] Bing Li,[1] Kewei Huang,[1] Chengwei Yang,[1] and Yimeng Jiang[2]

[1]*School of Mechatronical Engineering, Beijing Institute of Technology, Beijing 100081, China*
[2]*China Academy of Launch Vehicle Technology, Beijing 100076, China*

Correspondence should be addressed to Chengwei Yang; yangchengwei2009@126.com

Received 5 January 2015; Accepted 11 June 2015

Academic Editor: Andrzej Swierniak

The trajectory of a tubular launched cruising unmanned aerial vehicle is optimized using the modified direct collocation method for attacking a target at back slope under a wind gradient. A mathematical model of the cruising unmanned aerial vehicle is established based on its operational and motion features under a wind gradient to optimize the trajectory. The motion characteristics of "altitude adjustment" and "suicide attack" are taken into full account under the combat circumstance of back slope time key targets. By introducing a discrete time function, the trajectory optimization is converted into a nonlinear programming problem and the SNPOT software is applied to solve for the optimal trajectory of the missile under different wind loads. The simulation results show that, for optimized trajectories, the average attack time decreased by up to 29.1% and the energy consumption is reduced by up to 25.9% under specified wind gradient conditions. A, ω_{dire}, and $W_{\max}$ have an influence on the flight trajectories of cruising unmanned aerial vehicle. This verifies that the application of modified direct collocation method is reasonable and feasible in an effort to achieve more efficient missile trajectories.

1. Introduction

Enemy armored vehicles, missile launchers, and support vehicles always use the favorable terrain to mask their location, such as a back slope. In modern warfare, however, it is not practical to cause effective damage in such situations, using conventional ammunition following its original trajectory. These types of targets can be effectively attacked through the best trajectory and attack strategy of a cruising unmanned aerial vehicle (CUAV) [1, 2]. Taking the tubular launched CUAV as an example, it will unfold and change to a conventional aircraft after launched by the tube for storage, transportation, and launch. After a short attitude adjustment, it will avoid mountains and obstacles rapidly and can attack time sensitive key targets at a back slope. A large number of studies on operational use and trajectory optimization of CUAVs have been conducted by scholars around the world. Reference [3] provided the optimal strategy for guiding a CUAV in reconnaissance and search during military operational procedures. In [4], the optimal ballistic trajectory problem of CUAV at attack stage with the adoption of genetic algorithm was solved. In [5], the operational efficiency of CUAV for attacking time sensitive key targets was studied. For trajectory planning, [6] determined the optimal path of small and medium-sized UAV attacking targets in urban warfare by application of TSP method. In [7], the optimal climbing trajectory for UAV through the study of UAV climbing performance was given. Reference [8] studied the shortest trajectory of small UAV spying on multiple targets through refueling. Reference [9] established a trajectory generation method of terrain following and threat avoidance for UAVs at low altitude. References [10, 11] presented the optimal strategy of multiple UAVs under cooperative search and attack. Considering the influence of wind field on UAV

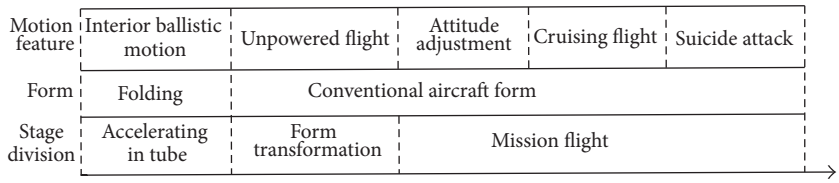

Figure 1: Operation process analysis of tubular launched CUAV.

flight performance and aiming at studying the effects of wind field on trajectory, references [12–16] studied the optimal trajectory of a small UAV when taking periodic motions in dynamic wind gradient field. In [17] the influences of wind power and solar energy on flight endurance of small UAV were studied. Reference [18] investigated the use of fuzzy logic in the flight trajectory of a UAV under the condition of known wind velocities. Reference [19] studied the influence of wind velocities between city buildings on the motion of a UAV. Reference [20] studied the optimal trajectory of a UAV collecting wind power through dynamic soaring. Considering that a CUAV combines both the characteristics of ammunition and a UAV, the features of unpowered gliding and posture adjustment as well as suicide attacks during the whole operation process should be fully included in the research of trajectory optimization.

In the present work, the motion features of portable tubular launched CUAV were first analyzed, and the kinematic and dynamic equations of CUAV dynamics at different stages under the background of attacking targets on a back slope were also analyzed according to ENU coordinate system. The model was discretized with a discrete time function according to constraint conditions such as initial position, terminal position, velocity, attitude, flight performance, and terrain and the solution was optimized by using software SNOPT. The optimal trajectory for attacking targets at back slope under different wind gradients and the methods in improving attack performance of CUAV by using wind gradient were studied.

2. Problem Description

Operating procedures of a portable tubular launched CUAV can be divided into three stages. The first stage is to provide enough initial kinetic energy with the aid of external input. The second is the form transformation stage, in which the CUAV enters into safety attitude with unpowered flight. The third stage is the mission flight.

After further analyses of the process, a diagram which takes time as the horizontal axis and CUAV features as the vertical axis was established. Based on the stage division, initial launching stage, unfolding stage, and mission stage were marked on the time axis, while the features of the CUAV were identified from motion features and form. To facilitate the systematic description of the process, we assumed that every feature is delineated instantaneously and the final analysis diagram is shown in Figure 1. According to the stage division, during the working process, the correspondence of time and CUAV form can be found. The CUAV keeps folding from the launch point to the unfolding point; after that the form transforms to conventional aircraft.

Form change of tubular launched CUAV will directly affect its motion features. Interior ballistic motion is performed in changing from the tube from the launch stage to the unfolding stage. When it unfolds, the CUAV first enters into a safety attitude in unpowered flight, and then both the control system and the dynamic system begin to work with the power supply and the missile adjusts its attitude according to the route defined by the trajectory planning. Finally it arrives at the target area and attacks enemy target.

Combat background here is as follows: one of the combat groups considered is at the foot of the mountain. A high altitude UAV detects that certain enemy time sensitive key target is masking its location somewhere at a back slope and its location becomes clear. The UAV sends the specific coordinates to the combat group. The mission is for the combat group to attack the target at the back slope with a tubular launched CUAV, which is equipped with a one-time use, low-cost ammunition. The objective function of trajectory optimization for CUAV is set as

$$\min J_{\text{time}} = t_e \tag{1}$$

in which t_e is the flight time after CUAV unfolds.

3. Mathematical Model

3.1. Model Assumptions

(1) Magnitude and direction of the wind velocity are only related to attitude h and are invariable over time.

(2) Quality of CUAV m is a constant and energy capacity of battery is enough to support the CUAV arriving in target area.

(3) Launching angle γ_0, initial launching velocity V_0 and form transformation time t_b of CUAV are fixed values as they are systematic design parameters.

(4) CUAV instantly unfolds when it is ejected from launch tube. The transformation process of "loader" is too fast to cause any influence on attitude.

3.2. Kinematic and Dynamical Models. Particle kinematic and dynamical models of CUAV were established from unfolding according to the division of stages.

(1) The initialization of the form transformation stage is at $(0, t_b)$, in which point the CUAV transitions to an unpowered flight stage. Particle kinematics and dynamics equations for this stage can be written as

$$\begin{aligned}
\dot{x} &= V\cos\gamma\sin\psi + W_x,\\
\dot{y} &= V\cos\gamma\cos\psi + W_y,\\
\dot{h} &= V\sin\gamma + W_h,\\
m\dot{V} &= -D_{\text{glider}} - mg\sin\gamma - m\dot{W}_x\cos\gamma\sin\psi\\
&\quad - m\dot{W}_y\cos\gamma\cos\psi - m\dot{W}_h\sin\gamma,\\
mV\cos\gamma\dot{\psi} &= -m\dot{W}_x\cos\psi + m\dot{W}_y\sin\psi,\\
mV\dot{\gamma} &= L_{\text{glider}} - mg\cos\gamma + m\dot{W}_x\sin\gamma\sin\psi\\
&\quad + m\dot{W}_y\sin\gamma\cos\psi - m\dot{W}_h\cos\gamma
\end{aligned} \tag{2}$$

in which h is the altitude, (x, y) are (east, north) position, V is the airspeed, ψ is the heading angle measured clockwise from the north, g is the acceleration of gravity, and L_{glider} and D_{glider} are lift and drag when cruising mission is unpowered flying. Define

$$\begin{aligned}
L_{\text{glider}} &= 0.5\rho V^2 S C_{L_{\text{glider}}},\\
D_{\text{glider}} &= 0.5\rho V^2 S C_{D_{\text{glider}}},
\end{aligned} \tag{3}$$

where $C_{L_{\text{glider}}}$ and $C_{D_{\text{glider}}}$ are the lift coefficient and the drag coefficient when cruising mission is unpowered flying, ρ is air density, and S is wing area.

(W_x, W_y, W_h) and $(\dot{W}_x, \dot{W}_y, \dot{W}_h)$ are wind speed and wind acceleration along the axis, respectively. Consider

$$\begin{aligned}
\dot{W}_x &= \frac{\partial W_x}{\partial x}\dot{x} + \frac{\partial W_x}{\partial y}\dot{y} + \frac{\partial W_x}{\partial h}\dot{h},\\
\dot{W}_y &= \frac{\partial W_y}{\partial x}\dot{x} + \frac{\partial W_y}{\partial y}\dot{y} + \frac{\partial W_y}{\partial h}\dot{h},\\
\dot{W}_h &= \frac{\partial W_h}{\partial x}\dot{x} + \frac{\partial W_h}{\partial y}\dot{y} + \frac{\partial W_h}{\partial h}\dot{h}.
\end{aligned} \tag{4}$$

(2) The mission flight time of CUAV is (t_b, t_e). Its kinematics equations can be conveyed by (2) and its dynamics equations can be written as follows:

$$\begin{aligned}
m\dot{V} &= T - D - mg\sin\gamma - m\dot{W}_x\cos\gamma\sin\psi\\
&\quad - m\dot{W}_y\cos\gamma\cos\psi - m\dot{W}_h\sin\gamma,\\
mV\cos\gamma\dot{\psi} &= L\sin\mu - m\dot{W}_x\cos\psi + m\dot{W}_y\sin\psi,\\
mV\dot{\gamma} &= L\cos\mu - mg\cos\gamma + m\dot{W}_x\sin\gamma\sin\psi\\
&\quad + m\dot{W}_y\sin\gamma\cos\psi - m\dot{W}_h\cos\gamma
\end{aligned} \tag{5}$$

in which T is the thrust from airscrew and L and D are lift and drag between t_b and t_e. We have

$$\begin{aligned}
L &= 0.5\rho V^2 S C_L,\\
D &= 0.5\rho V^2 S C_D,
\end{aligned} \tag{6}$$

where C_L and C_D are lift coefficient and the drag coefficient between t_b and t_e. C_D can be determined from

$$C_D = C_{D0} + C_{D1}C_L + C_{D2}C_L^2 \tag{7}$$

in which C_{D0} is the parasitic drag coefficient and C_{D1} and C_{D2} are constants defining a drag polar. Other variables are as listed above.

V_{inertial} is ground velocity of CUAV and is defined as

$$V_{\text{inertial}} = \sqrt{\dot{x}^2 + \dot{y}^2 + \dot{h}^2}. \tag{8}$$

The state variables of CUAVs in (2) and (6) are $\begin{bmatrix} V & \psi & \gamma & x & y & h \end{bmatrix}'$ and the control variables are $\begin{bmatrix} C_L & \mu & T \end{bmatrix}'$. According to the model assumptions, the position and posture of the CUAV at t_b can be described as follows:

$$\boldsymbol{\Gamma}_{t_b} = \boldsymbol{\Gamma}_0 + \int_0^{t_b} \dot{\boldsymbol{\Gamma}} dt, \tag{9}$$

where $\boldsymbol{\Gamma}$ are the state variables.

3.3. Formal Modeling in Battlefield Environment. The battlefield environment includes factors such as the terrain, climate, and hydrology. According to the requirements of mission operation, the operational mountain discrete model and airspace gradient wind model were established.

3.3.1. Discrete Mountain Model. The three-dimensional terrain of mountain is shown in Figure 2. A cube area ABCD-EFGH was first built, which completely covered the mountain area, as shown in Figure 3. The area was divided into m and n sections along the x-and y-axes, respectively. These sections and three-dimensional figures cross each other and form $m \times n$ point coordinates, so that the three-dimensional terrain is discretized into a $m \times n$ grid. Space coordinates $(x_{Ti,j}, y_{Ti,j}, h_{Ti,j})$ for each grid represent position and height of the point.

3.3.2. Wind Velocity Model in Operation Airspace. Actual wind velocity changes according to a linear gradient, wind index or logarithm [21]. The wind speed is given by

$$W = \frac{W_{\max}}{h_{\max}}\left[Ah + \frac{1-A}{h_{\max}}h^2\right], \tag{10}$$

where $W_{\max}$ is the maximum value of wind, $h_{\max}$ is the maximum value of flight altitude, and A is the type of wind gradient.

If $A = 1$, the profile of wind velocity changes as a straight line; if $0 \le A < 1$, it changes according to similar index; if $1 < A \le 2$, the profile changes according to the similar logarithm, as shown in Figure 4.

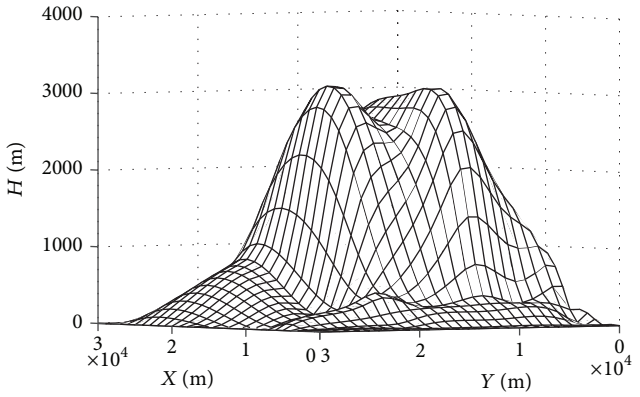

Figure 2: Three-dimensional mountain model.

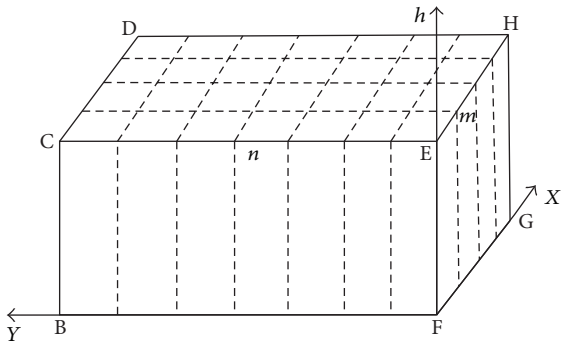

Figure 3: Discretization of model.

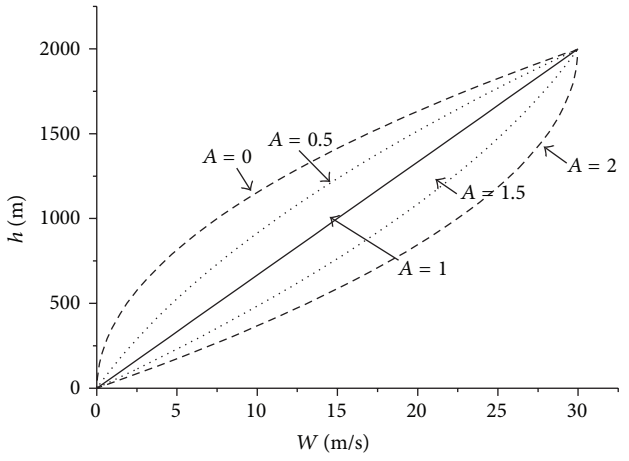

Figure 4: Wind profile changes.

To simplify (11), here we set

$$\beta = \frac{W_{\max}}{h_{\max}}. \tag{12}$$

Then the wind gradient model can be simplified as

$$W = \beta\left[Ah + \frac{1-A}{h_{\max}}h^2\right], \quad (0 \le A \le 2). \tag{13}$$

Assuming that ω_{dire} is the wind direction angle between the wind direction and the y-axis direction, then

$$\begin{aligned} W_x &= W * \sin\omega_{\text{dire}}, \\ W_y &= W * \cos\omega_{\text{dire}}, \\ W_h &= 0. \end{aligned} \tag{14}$$

3.4. Constraint Condition. (1) Initial position constraint conditions are

$$\begin{aligned} x(0) &= x_0, \\ y(0) &= y_0, \\ h(0) &= h_0, \\ V(0) &= V_0, \\ \gamma(0) &= \gamma_0, \end{aligned} \tag{15}$$

where x_0, y_0, and h_0 denote the unfolding point coordinates when launching the CUAV; V_0 and γ_0 refer to the velocity and launching angle of CUAV ejecting from launch tube, respectively.

(2) Terminal position constraint conditions are

$$\begin{aligned} \left|x(t_e) - x_{t_e}\right| &\le \Delta x, \\ \left|y(t_e) - y_{t_e}\right| &\le \Delta y, \\ \left|h(t_e) - h_{t_e}\right| &\le \Delta h, \\ V(t_e) &= V_{t_e}, \\ \gamma(t_e) &= \gamma_{t_e}, \end{aligned} \tag{16}$$

where $(x_{t_e}, y_{t_e}, h_{t_e})$ denotes the position coordinates for back slope target; Δx, Δy, and Δh are the allowable deviation in the position from the terminal attack point; V_{t_e} and γ_{t_e} are velocity and attitude constraints to terminal attack of CUAV.

(3) Process constraint conditions are

$$\begin{aligned} &x_{\min} \le x(t) \le x_{\max}, \\ &y_{\min} \le y(t) \le y_{\max}, \\ &h_{\min} \le h(t) \le h_{\max}, \\ &V_{\min} \le V(t) \le V_{\max}, \\ &\gamma_{\min} \le \gamma(t) \le \gamma_{\max}, \\ &\psi_{\min} \le \psi(t) \le \psi_{\max}, \\ &0 \le P(t) \le P'_{\max}\eta_{\text{prop}}, \\ &\dot{\gamma}_{\min} \le \dot{\gamma}(t) \le \dot{\gamma}_{\max}, \\ &\dot{\psi}_{\min} \le \dot{\psi}(t) \le \dot{\psi}_{\max}, \\ &\left\|x(t) - x_{Ti,j}, y(t) - y_{Ti,j}, h(t) - h_{Ti,j}\right\|_2 \ge R_{Ti,j} \\ &\qquad (i = 1, 2, \ldots, m;\ j = 1, 2, 3, \ldots, n). \end{aligned} \tag{17}$$

Equation (17) is the flight performance and mountain obstacle constraints, in which $x(t)$, $y(t)$, $h(t)$, $V(t)$, $\gamma(t)$, $P(t)$, $\psi(t)$, $\dot{\gamma}(t)$, and $\dot{\psi}(t)$ represent position, velocity, flight path angle, propeller power, flight path drift angle, change rate of flight path angle, and change rate of flight path drift angle when the CUAV is at time t, respectively. Also, $V(t)$, $\gamma(t)$, $P(t)$, and $\psi(t)$ are the limitation on flight performance. $\dot{\gamma}(t)$ and $\dot{\psi}(t)$ are the limitation on the performance of maneuverability. In the following table, min and max, respectively, refer to the corresponding allowable minimum and maximum parameters; $P'_{\max}$ is the maximum power of battery; η_{prop} is the efficiency of battery power converting to propeller thrust power, which is specified as 0.6 [16]; $\|\cdot\|_2$ represents the distance between two points, and $(x_{Ti,j}, y_{Ti,j}, h_{Ti,j})$ and $R_{Ti,j}$ are coordinates of discrete points and safe flight distance, respectively.

(4) Control variable constraint conditions are

$$\begin{aligned} C_{L_{\min}} \le C_L(t) \le C_{L_{\max}} \\ \mu_{\min} \le \mu(t) \le \mu_{\max} \\ 0 \le T(t) \le T_{\max}. \end{aligned} \tag{18}$$

4. Modified Direct Collocation Method

Direct collocation method is one of main methods employed in trajectory optimization research. It generally divides the whole system course into equal N segments and two endpoints of each segment which describes the changes of state variables over time with polynomial. It assumes that the change of control variables is linear [21] and the tubular launched CUAVs have the motion features of attitude adjustment and suicide attack. If we use the conventional average discrete method, the discrete model will be weakened or even the two motion features will be lost. Therefore, the time discrete function was established here for the CUAV and Simpson method was used on polynomial. The basic steps are listed as follows:

(1) Time course was discretized; namely,

$$t_b = t_0 < t_1 < t_2 < \cdots < t_N = t_e. \tag{19}$$

The corresponding state variables and control variables to time points can be, respectively, recorded as $(X_0, X_1, \ldots, X_N)$ and $(U_0, U_1, \ldots, U_N)$. Discrete function of time is as follows:

$$\begin{aligned} \kappa_{i+1} &= t_{i+1} - t_i \\ &= \lambda * e^{(-(i+1-\xi)^2/\varepsilon)} * \frac{t_e - t_b}{\sum_{j=1}^{N} \lambda * e^{(-(j-\xi)^2/\varepsilon)}} \\ &\qquad i = 0, 1, 2, \ldots, N-1, \end{aligned} \tag{20}$$

where λ and ε are discrete point distribution factor; ξ is time discrete symmetry factor.

(2) Each state variable was expressed with cubic Hermit polynomial on its subinterval:

$$X = c_0 + c_1 s + c_2 s^2 + c_3 s^3, \tag{21}$$

$s = (t - t_i)/\kappa_i$, and $s \in [0, 1]$, in which boundary conditions can be obtained as follows:

$$\begin{aligned} X_1 &= X(0), \\ X_2 &= X(1), \\ \dot{X}_1 &= \left.\frac{dX}{ds}\right|_{s=0}, \\ \dot{X}_2 &= \left.\frac{dX}{ds}\right|_{s=1} \end{aligned} \tag{22}$$

and then

$$\begin{bmatrix} X_1 \\ \dot{X}_1 \\ X_2 \\ \dot{X}_2 \end{bmatrix} = \begin{bmatrix} 1 & 0 & 0 & 0 \\ 0 & 1 & 0 & 0 \\ 1 & 1 & 1 & 1 \\ 0 & 1 & 2 & 3 \end{bmatrix} \begin{bmatrix} c_0 \\ c_1 \\ c_2 \\ c_3 \end{bmatrix}. \tag{23}$$

To solve it, we can obtain

$$\begin{bmatrix} c_0 \\ c_1 \\ c_2 \\ c_3 \end{bmatrix} = \begin{bmatrix} 1 & 0 & 0 & 0 \\ 0 & 1 & 0 & 0 \\ -3 & -2 & 3 & -1 \\ 2 & 1 & -2 & 1 \end{bmatrix} \begin{bmatrix} X_1 \\ \dot{X}_1 \\ X_2 \\ \dot{X}_2 \end{bmatrix}. \tag{24}$$

According to above equations, the polynomial expressing the corresponding state can be solved based on the given state variables at the node of each group. The collocation point was defined as the midpoint of subinterval, $s = 1/2$, and now

$$\begin{aligned} X_{ci} &= \frac{X_i + X_{i+1}}{2} + \frac{\kappa_i}{8}(f_i - f_{i+1}), \\ X'_{ci} &= -\frac{3(X_i + X_{i+1})}{2\kappa_i} - \frac{f_i + f_{i+1}}{4}, \end{aligned} \tag{25}$$

where f_i is (2) and (6) evaluated at X_i.

$$f_i = f(X_i, U_i, t_i). \tag{26}$$

(3) In order to improve the cubic polynomial fit to the change of state variables, the derivative f_{ci} at the collocation point on the subinterval should be equal to X'_{ci} calculated from polynomial:

$$\Delta_i = f_{ci} - X'_{ci} = f_{ci} + \frac{3(X_i + X_{i+1})}{2\kappa_i} + \frac{f_i + f_{i+1}}{4} = 0. \tag{27}$$

Table 1: Other parameters of loiter munition and environmental parameters.

Parameters	Values
m (kg)	1.8
S (m^2)	0.1
ρ (kg/m^3)	1.23
C_{D0}	0.08258
C_{D1}	−0.176
C_{D2}	0.312
$h_{\max}$ (m)	2000

The mathematical model of the CUAV was first discretized by adding a discrete time function and then the nonlinear programming problem was solved by using SNOPT in the Matlab software package with the established constraint conditions taken into account.

5. Simulation Calculation and Results Analysis

5.1. Simulation Parameter Setting

Initial position constraint is

$$\begin{aligned}&[x(0), y(0), h(0), V(0), \gamma(0), t_b]\\&= [0, 0, 0, 40, 0.707, 1];\end{aligned} \tag{28}$$

terminal position constraint is

$$\begin{aligned}&\left[x_{t_e}, y_{t_e}, h_{t_e}, V_{t_e}, \gamma_{t_e}, \Delta x, \Delta y, \Delta h\right]\\&= [15000, 20000, 500, 30, -0.523, 0, 0, 0];\end{aligned} \tag{29}$$

process constraint is

$$\begin{aligned}-10000\,\text{m} \le x(t) \le 20000\,\text{m};\\-10000\,\text{m} \le y(t) \le 40000\,\text{m};\\30\,\text{m} \le h(t) \le 2000\,\text{m};\\10\,\text{m/s} \le V(t) \le 50\,\text{m/s};\\-1.31\,\text{rad} \le \gamma(t) \le 1.31\,\text{rad};\\-3.14\,\text{rad} \le \psi(t) \le 3.14\,\text{rad};\\0\,\text{W} \le P(t) \le 600\,\text{W};\\-0.52\,\text{rad/s} \le \dot{\gamma}(t) \le 0.52\,\text{rad/s};\\-0.52\,\text{rad/s} \le \dot{\psi}(t) \le 0.52\,\text{rad/s};\end{aligned} \tag{30}$$

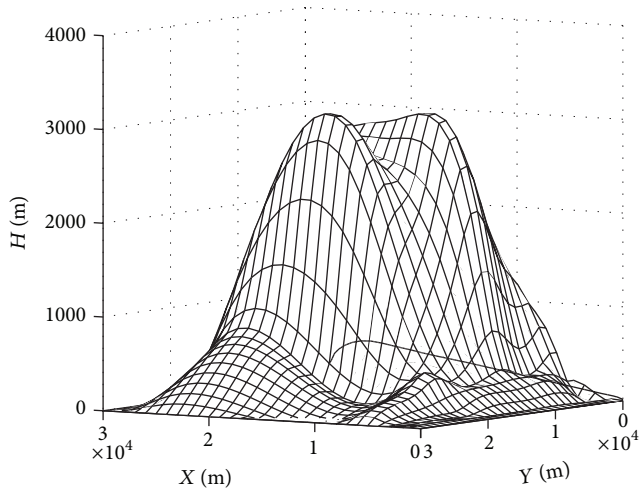

Figure 5: Operational flight trajectory of the CUAV ($W_{\max} = 0$ m/s).

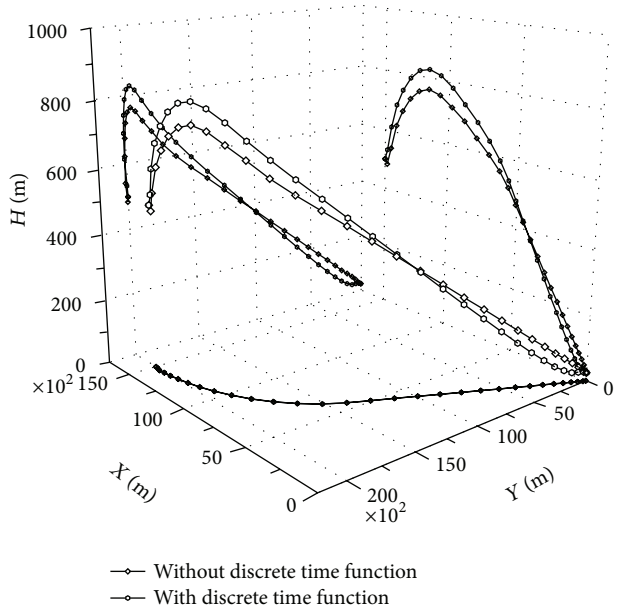

Figure 6: Influence of discrete time function on the trajectory.

control variable constraint is

$$\begin{aligned}-0.2 \le C_L \le 1.2;\\-1.57\,\text{rad} \le \mu(t) \le 1.57\,\text{rad};\\0\,\text{N} \le T(t) \le 12\,\text{N};\end{aligned} \tag{31}$$

the time discrete function was set as

$$\begin{aligned}&[\lambda, \xi, \varepsilon] = [0.05, 15.5, 128];\\&N = 30.\end{aligned} \tag{32}$$

Other parameters of CUAV and environmental parameters are shown in Table 1.

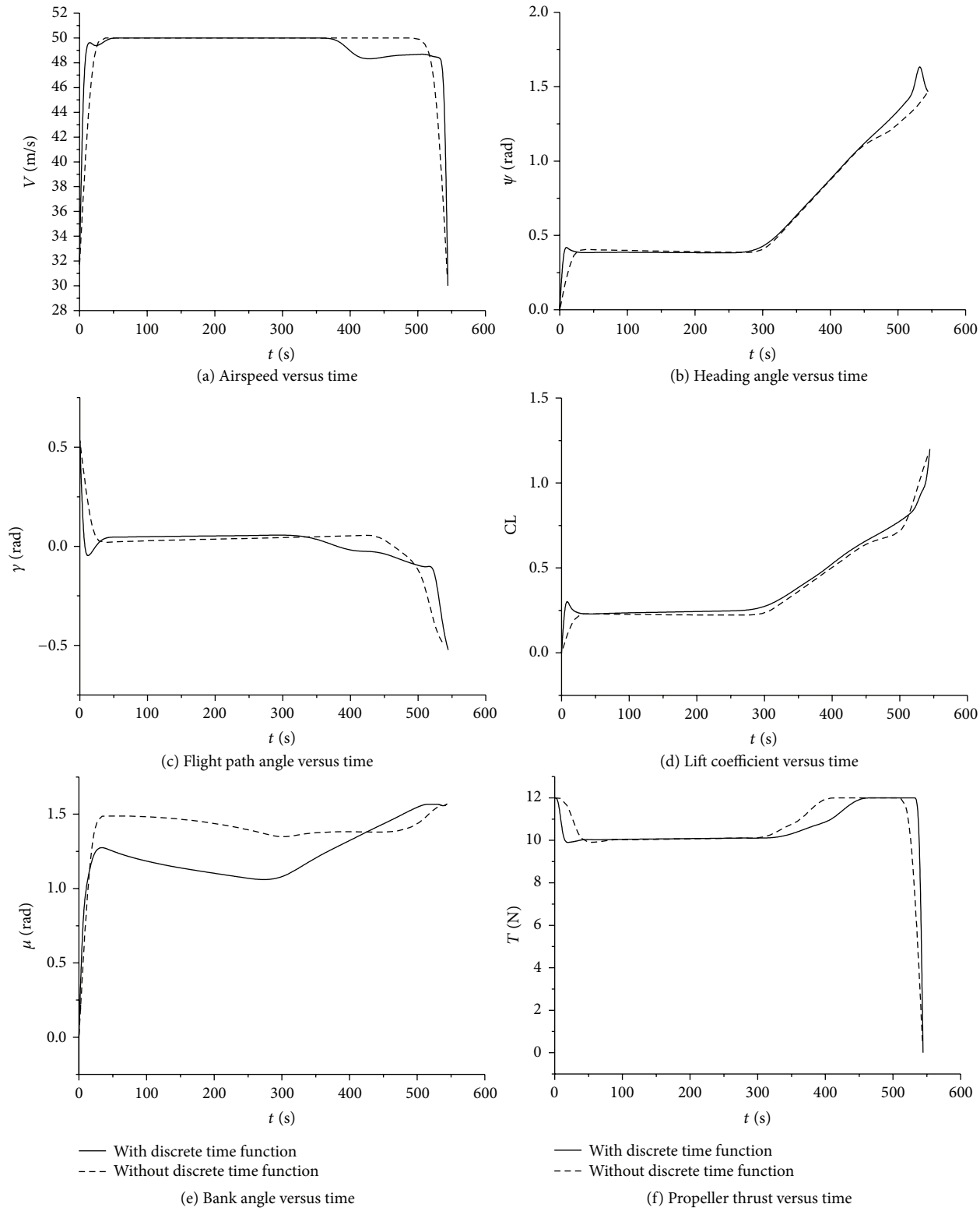

(a) Airspeed versus time
(b) Heading angle versus time
(c) Flight path angle versus time
(d) Lift coefficient versus time
(e) Bank angle versus time
(f) Propeller thrust versus time

Figure 7: Changing curve of state variable and control variable (W_{max} = 0 m/s).

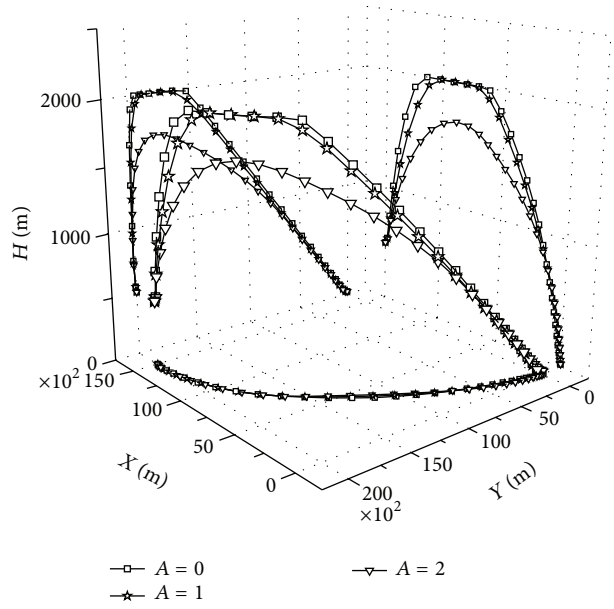

Figure 8: CUAV flight trajectories ($W_{\max} = 30$ m/s, $\omega_{\text{dire}} = \pi/2$ rad).

5.2. Result and Analysis. The simulation was performed on a 2.6 GHz PC and algorithm is real-time as computation time is 21 s under Matlab environment. As can be observed from Figure 5, the generated trajectory is smooth, so that the CUAV can attack target avoiding mountain obstacles. From Figures 6~7, it can be seen that the optimized trajectory has obvious features of attitude adjustment and suicide attack after adding the discrete time function. When the CUAV unfolds, an attitude adjustment stage is clearly showed and the attitude is adjusted to maximum velocity 50 m/s. When CUAV adjusts to cruising state, it climbs steadily and closes to the target around mountain obstacle. At the end of attack stage there is a clear dive-hike process and the flight speed is adjusted to terminal constraints velocity 30 m/s. The trajectory without time discrete function loses the attitude adjustment information in the initial stage and the information reflecting attitude and control in suicide attack stage is less. The results indicate that discrete time function is effective and its related discretized model contains more motion features of CUAVs.

The optimal trajectories of attack under wind gradient and without wind are quite different. As shown in Figures 8~9, the CUAV can avoid mountain obstacles and climb with smaller flight path drift angle ψ at the beginning of attack trajectory. It climbs to maximum altitude 2000 m at about 300 s and then increases the flight path drift angle. At this point ground velocity of CUAV obviously increases under the influence of wind speed, up to nearly 75 m/s as shown in Figures 10~11. The CUAV can avoid obstacles and keep at 2000 m height. When it gets close to the target, it dives and attacks it.

Table 2: Influence of wind gradient on attack time and energy consumption.

	$A = 0$	$A = 1$	$A = 2$	Average
Q	11.84%	13.34%	17.4%	13.3%
I	6.94%	7.72%	8.51%	7.72%

In order to analyze the influence of the gradient in wind speed on attack time, here influence function Q is obtained as follows:

$$Q = \frac{J_0 - J_W}{J_0} \times 100\%, \tag{33}$$

where J_0 is the attack time for CUAV without wind gradient and J_W is the attack time under wind gradient (Figure 16). Similarly the influence function I of wind to energy consumption can be defined.

As shown in Table 2, when $W_{\max} = 30$ m/s and $\omega_{\text{dire}} = \pi/2$ rad, attack time of the CUAV attacking target can be reduced by 13.3% on average and energy consumption reduced by 7.72%.

The flight trajectories at different of wind direction angles and maximum values of wind are summarized in order to further analyze the influence of battlefield environment on the CUAV flight trajectory.

Figure 12 presents the flight trajectories of CUAV for different wind direction angles when $W_{\max} = 30$ m/s and $A = 1$. Figure 13 shows the influence of wind direction angle on the attack time and energy consumption, and when $\omega_{\text{dire}} = 45^\circ$, the attack time and energy consumption of CUAV

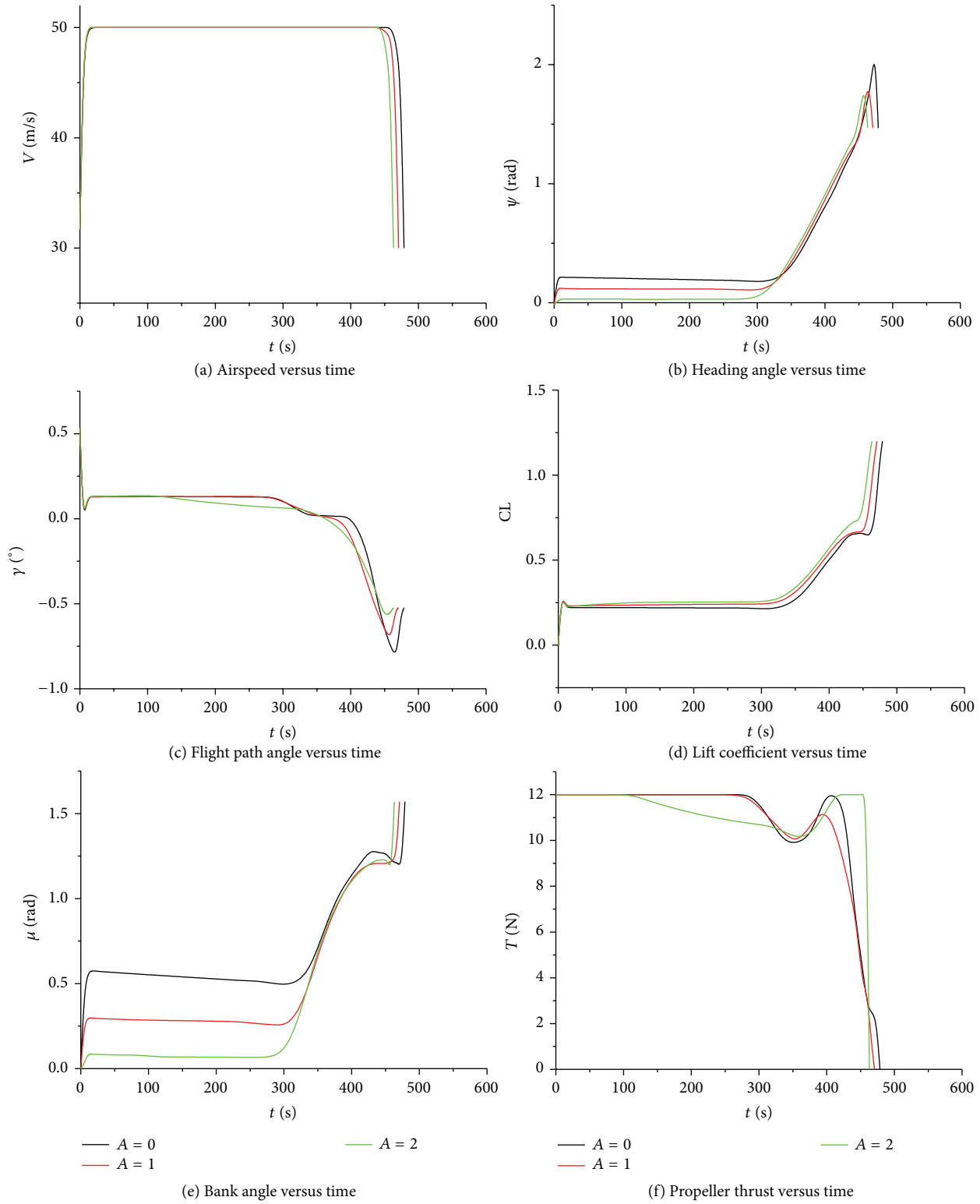

(a) Airspeed versus time

(b) Heading angle versus time

(c) Flight path angle versus time

(d) Lift coefficient versus time

(e) Bank angle versus time

(f) Propeller thrust versus time

Figure 9: Changing curve of state variable and control variable variables (W_{max} = 30 m/s, ω_{dire} = $\pi/2$ rad).

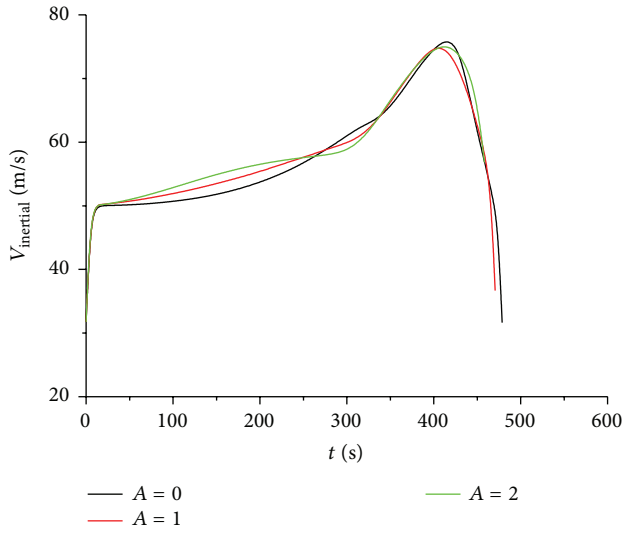

Figure 10: Inertial speed versus time.

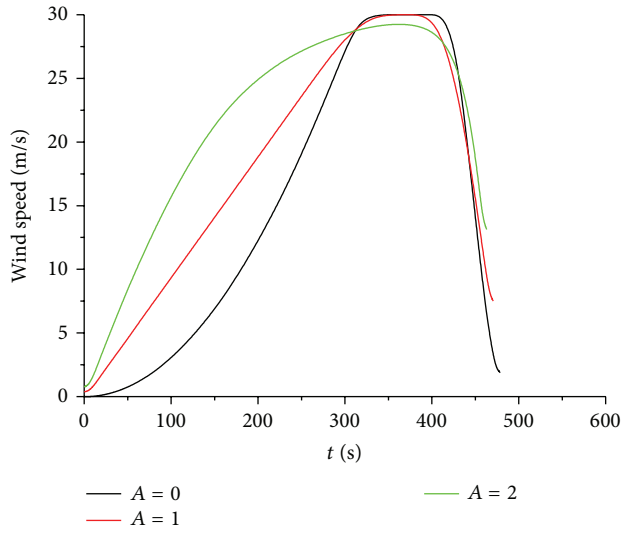

Figure 11: Wind speed versus time.

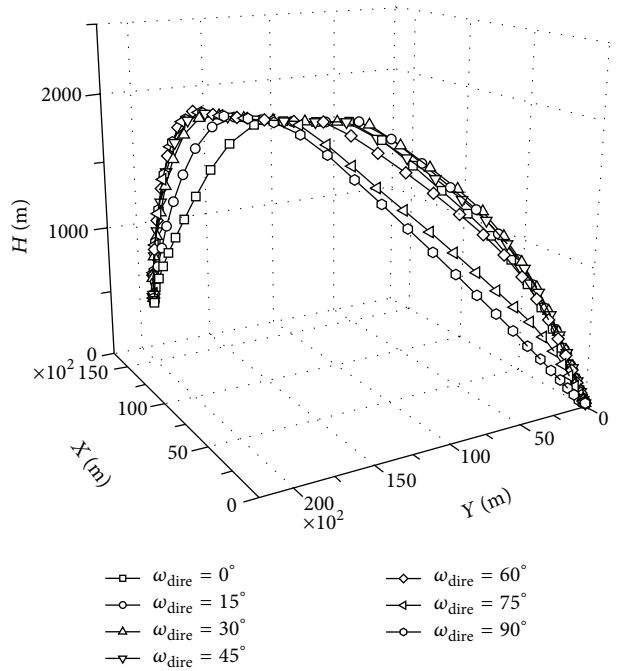

Figure 12: CUAV flight trajectories of different wind direction angles.

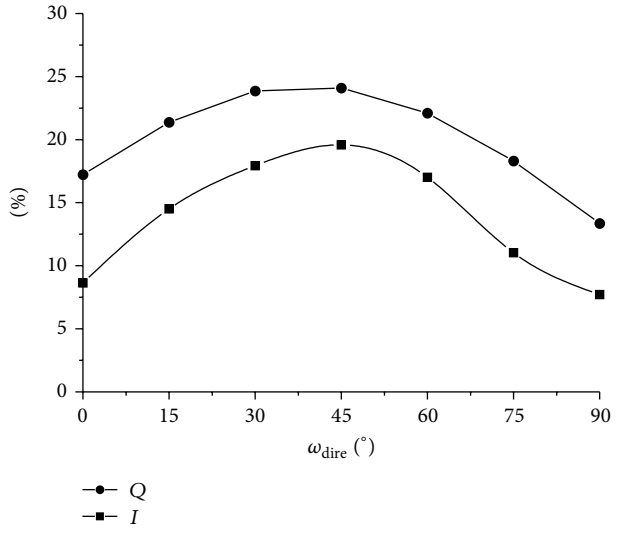

Figure 13: Influence of ω_{dire} on the attack time and energy consumption.

can decrease 24.1% and 19.6%, respectively. The changes of state variable and control variable variables for different wind direction angles are shown in Figure 14.

Figure 15 presents the flight trajectories of CUAV for different maximum values of wind when $\omega_{\text{dire}} = 45^\circ$ and $A = 1$. Obviously, there have obvious difference between the trajectories with and without wind gradient. But the changes of $W_{\max}$ have less influence on the flight trajectory when $5 \leq W_{\max} \leq 40$ m/s. The attack time and energy consumption of CUAV can decrease 29.1% and 25.9%, respectively. The changes of state variable and control variable variables for different maximum values of wind are shown in Figure 17.

6. Conclusion

In the present work, the operational processes of a tubular launched CUAV were analyzed, and the mathematical model for describing the dynamics was established for a missile attacking time sensitive key targets at a back slope under wind loading. In view of the motion features of attitude adjustment and suicide attack for tubular launched CUAVs, a discrete time function was added in the direct collocation

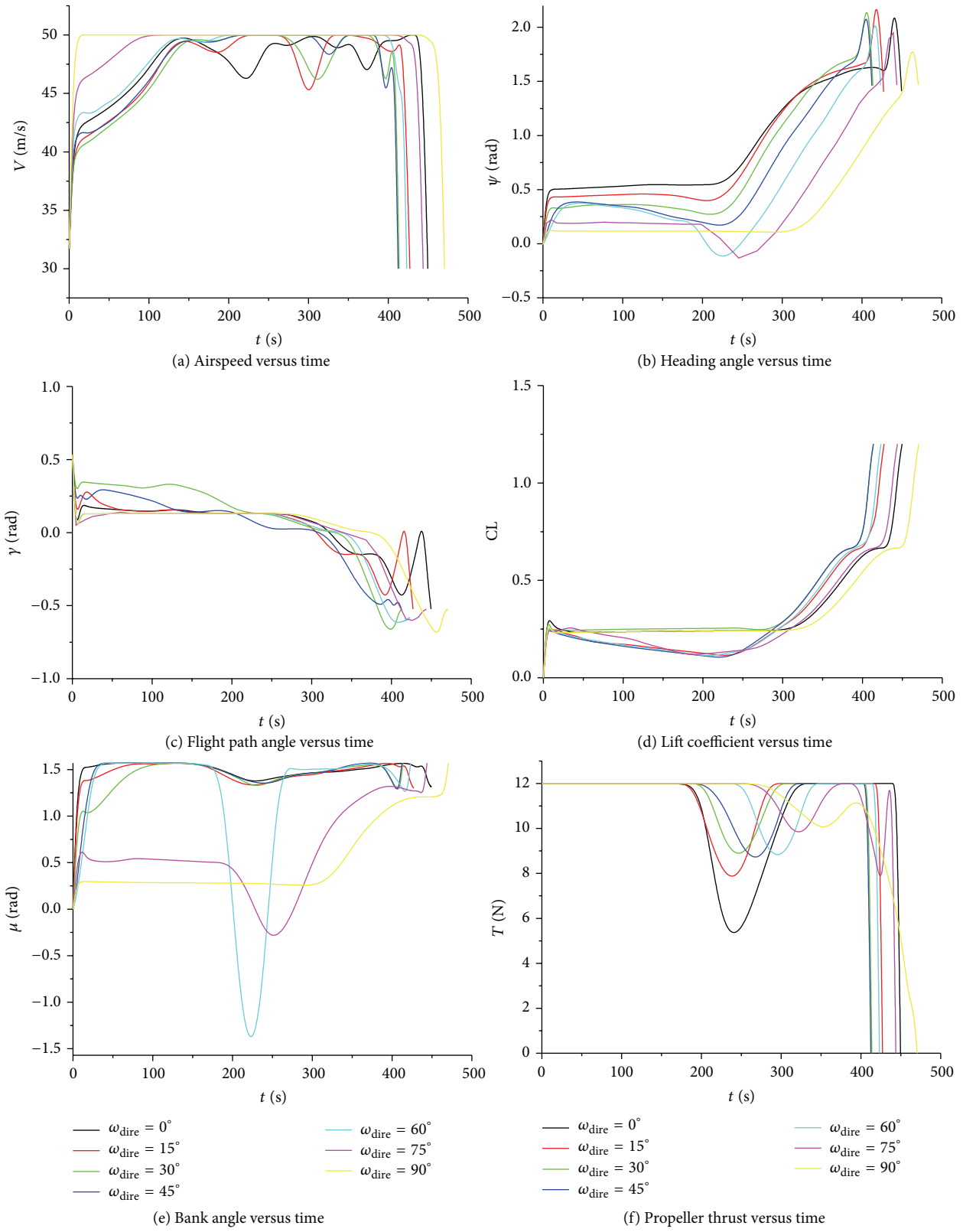

(a) Airspeed versus time

(b) Heading angle versus time

(c) Flight path angle versus time

(d) Lift coefficient versus time

(e) Bank angle versus time

(f) Propeller thrust versus time

FIGURE 14: Changing curve of state variable and control variable variables at different ω_{dire}.

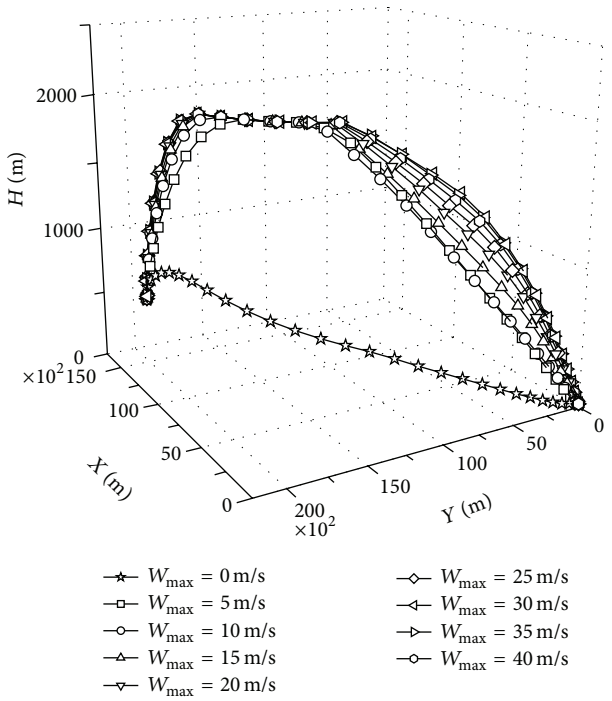

Figure 15: CUAV flight trajectories for different maximum values of wind.

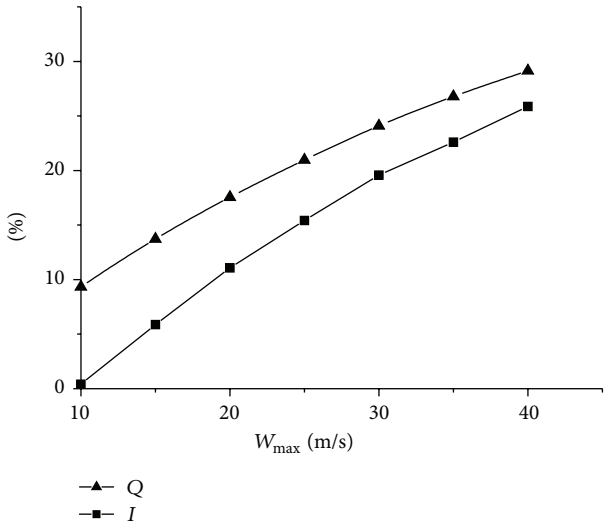

Figure 16: Influence of W_{max} on attack time and energy consumption.

method. In this way, the problem was converted into a nonlinear programming problem and then the CUAV trajectory was optimized by using the software SNOPT. Simulation results indicate that this method can effectively keep the motion features of attitude adjustment and suicide attack. The simulation results show that, for optimized trajectories, the average attack time decreased by up to 29.1% and the energy consumption is reduced by up to 25.9% under specified wind gradient conditions, which has an important significance in enriching and perfecting the operational use of CUAV.

Conflict of Interests

The authors declare that there is no conflict of interests regarding the publication of this paper.

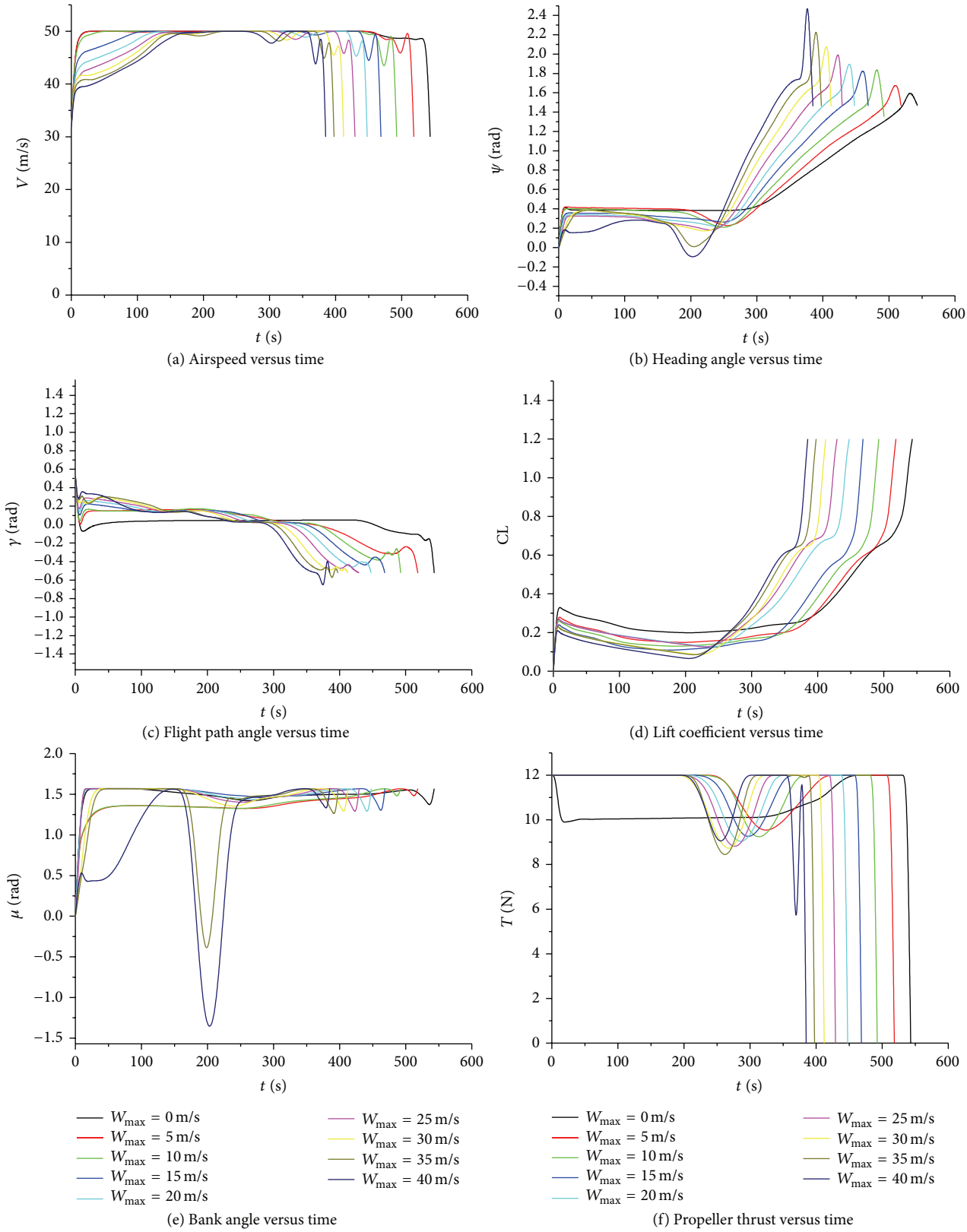

Figure 17: Changing curve of state variable and control variable variables for different maximum values of wind.

References

[1] X.-L. Ji and G.-L. He, "Aerodynamic characteristics of gun-launched loitering munitions and its shape design," *Transaction of Beijing Institute of Technology*, vol. 28, no. 11, pp. 953–961, 2008 (Chinese).

[2] B. Li, J. Li, G. He, and D. Li, "Research on cooperative combat for integrated reconnaissance-attack-BDA of group LAVs," *Mathematical Problems in Engineering*, vol. 2014, Article ID 123142, 6 pages, 2014.

[3] M.-F. Guo, N.-J. Fan, and Z.-H. Yuan, "Battlefield operational strategy of loitering munition," *Acta Armamentarii*, vol. 27, no. 5, pp. 944–947, 2006 (Chinese).

[4] Y. Wang, D. Li, and Q. Shen, "Path Planning for the attack stage of a loitering unit," *Transactions of Beijing Institute of Technology*, vol. 28, no. 1, pp. 8–10, 2008 (Chinese).

[5] X.-L. Ji, D.-L. Li, and G.-L. He, "Combat efficiency analyses for loitering missile attacking time-critical target," *Transaction of Beijing Institute of Technology*, vol. 30, no. 1, pp. 46–49, 2010 (Chinese).

[6] T. Shima, S. Rasmussen, and D. Gross, "Assigning micro UAVs to task tours in an urban terrain," *IEEE Transactions on Control Systems Technology*, vol. 15, no. 4, pp. 601–612, 2007.

[7] P. Zhang, X. Wang, and X. Chen, "Climb trajectory optimization of UAV based on improved particle swarm optimization," *Computer Simulation*, vol. 29, no. 4, pp. 92–94, 2012 (Chinese).

[8] K. Sundar and S. Rathinam, "Algorithms for routing an unmanned aerial vehicle in the presence of refueling depots," *IEEE Transactions on Automation Science and Engineering*, vol. 11, no. 1, pp. 287–294, 2014.

[9] R. Zardashti, A. A. Nikkhah, and M. J. Yazdanpanah, "Constrained optimal terrain following/threat avoidance trajectory planning using network flow," *Aeronautical Journal*, vol. 118, no. 1203, pp. 523–539, 2014.

[10] H.-F. Guo, D.-L. Ding, W.-C. Wu, and Y.-L. Liu, "Long-range penetration and cooperative search decision-making of multiple UAVs," *Acta Armamentarii*, vol. 35, no. 2, pp. 248–255, 2014 (Chinese).

[11] C.-L. Tang, C.-Q. Huang, H.-W. Du, H.-Q. Huang, D.-L. Ding, and C. Luo, "Study of trajectory planning for UCAV formation cooperative attack," *Acta Armamentarii*, vol. 35, no. 4, pp. 523–530, 2014 (Chinese).

[12] Y. J. Zhao, "Optimal patterns of glider dynamic soaring," *Optimal Control Applications and Methods*, vol. 25, no. 2, pp. 67–89, 2004.

[13] Y. J. Zhao, "Taking advantage of wind energy in UAV operations," in *Proceedings of the InfoTech at Aerospace: Advancing Contemporary Aerospace Technologies and Their Integration*, pp. 26–29, American Institute of Aeronautics and Astronautics, Arlington,Va, USA, 2005.

[14] Y. J. Zhao, "Extracting energy from downdraft to enhance endurance of uninhabited aerial vehicles," *Journal of Guidance, Control, and Dynamics*, vol. 32, no. 4, pp. 1124–1133, 2009.

[15] H. Y. Singhania, *Practical strategies of wind energy utilization for uninhabited aerial vehicles in loiter flights [Ph.D. thesis]*, The University of Minnesota, Minnesota, Minn, USA, 2008.

[16] W. Guo, Y. J. Zhao, and B. Capozzi, "Optimal unmanned aerial vehicle flights for seeability and endurance in winds," *Journal of Aircraft*, vol. 48, no. 1, pp. 305–314, 2011.

[17] G. C. Bower, T. C. Flanzer, and I. M. Kroo, "Conceptual design of a small UAV for continuous flight over the ocean," in *Proceedings of the 11th AIAA Aviation Technology, Integration, and Operations Conference (ATIO '11)*, pp. 1–17, American Institute of Aeronautics and Astronautics, Virginia Beach, Va, USA, 2011.

[18] G. P. Kladisa, J. T. Economoua, K. Knowlesa, J. Lauberb, and T.-M. Guerra, "Energy conservation based fuzzy tracking for unmanned aerial vehicle missions under a priori known wind information," *Engineering Applications of Artificial Intelligence*, vol. 24, no. 2, pp. 278–294, 2011.

[19] C. White, E. W. Lim, S. Watkins, A. Mohamed, and M. Thompson, "A feasibility study of micro air vehicles soaring tall buildings," *Journal of Wind Engineering and Industrial Aerodynamics*, vol. 103, no. 1, pp. 41–49, 2012.

[20] V. Bonnin and C. C. Toomer, "Energy-harvesting mechanisms for UAV flight by dynamic soaring," in *Proceedings of the AIAA Atmospheric Flight Mechanics Conference (AFM '13)*, pp. 732–745, American Institute of Aeronautics and Astronautics, Boston, Mass, USA, 2013.

[21] C. R. Hargraves and S. W. Paris, "Direct trajectory optimization using nonlinear programming and collocation," *Journal of Guidance, Control, and Dynamics*, vol. 10, no. 4, pp. 338–342, 1987.